Article

High Purity Anatase TiO Nanocrystals: Near Room-Temperature Synthesis, Grain Growth Kinetics, and Surface Hydration Chemistry

Guangshe Li, Liping Li, Juliana Boerio-Goates, and Brian F. Woodfield

J. Am. Chem. Soc., **2005**, 127 (24), 8659-8666• DOI: 10.1021/ja050517g • Publication Date (Web): 27 May 2005

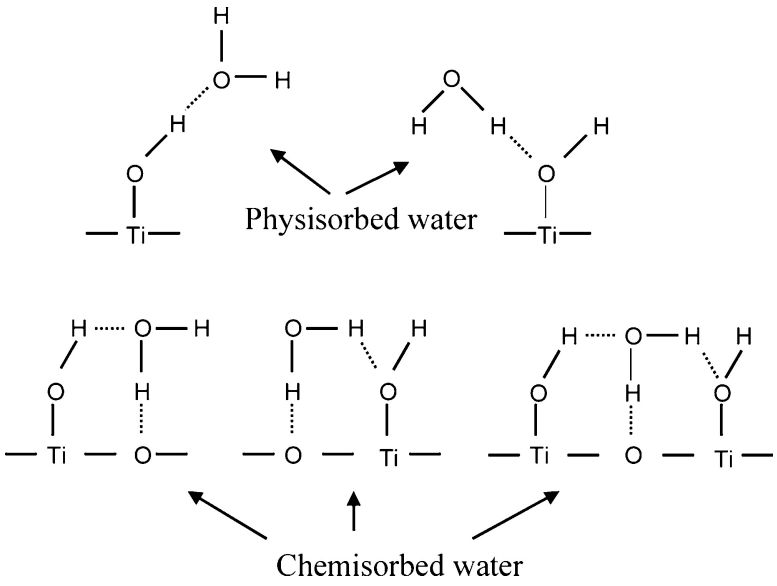

More About This Article

Additional resources and features associated with this article are available within the HTML version:

- Supporting Information
- Links to the 25 articles that cite this article, as of the time of this article download
- Access to high resolution figures
- Links to articles and content related to this article
- Copyright permission to reproduce figures and/or text from this article

View the Full Text HTML

J|A|C|S
ARTICLES
Published on Web 05/27/2005

High Purity Anatase TiO_2 Nanocrystals: Near Room-Temperature Synthesis, Grain Growth Kinetics, and Surface Hydration Chemistry

Guangshe Li,[†] Liping Li,[†] Juliana Boerio-Goates,[‡] and Brian F. Woodfield*[,‡]

Contribution from the Department of Chemistry and Biochemistry, Brigham Young University, Provo, Utah 84602, and State Key Lab of Structural Chemistry, Fujian Institute of the Research on the Structure of Matter, Chinese Academy of Sciences, Fuzhou, Fujian 350002, P. R. China

Received January 26, 2005; E-mail: Brian_Woodfield@byu.edu

Abstract: High purity, spherical anatase nanocrystals were prepared by a modified sol−gel method. Mixing of anhydrous $TiCl_4$ with ethanol at about 0 °C yielded a yellowish sol that was transformed into phase-pure anatase of 7.7 nm in size after baking at 87 °C for 3 days. This synthesis route eliminates the presence of fine seeds of the nanoscale brookite phase that frequently occurs in low-temperature formation reactions and also significantly retards the phase transformation to rutile at high temperatures. Heating the as-is 7.7 nm anatase for 2 h at temperatures up to 600 °C leads to an increase in grain size of the anatase nanoparticles to 32 nm. By varying the calcination time from 2 to 48 h at 300 °C, the particle size could be controlled between 12 and 15.3 nm. The grain growth kinetics of anatase nanoparticles was found to follow the equation, $D^2 - D_0^2 = k_0 t^m e^{(-E_a/RT)}$ with a time exponent $m = 0.286(\pm 9)$ and an activation energy of $E_a = 32 \pm 2$ kJ·mol^{-1}. Thermogravimetric analysis in combination with infrared and X-ray photoemission spectroscopies has shown the anatase nanocrystals at different sizes to be composed of an interior anatase lattice with surfaces that are hydrogen-bonded to a wide set of energetically nonequivalent groups. With a decrease in particle size, the anatase lattice volume contracts, while the surface hydration increases. The removal of the surface hydration layers causes coarsening of the nanoparticles.

Introduction

TiO_2 occurs in nature in three distinct crystallographic phases: anatase, brookite, and rutile,[1] and various forms of TiO_2 have found many important technological applications.[2] Among these polymorphs, TiO_2 in the anatase structure has been used as an excellent photocatalyst for photodecomposition and solar-energy conversion due to its high photoactivity.[3,4] Recent photocatalytic studies by Almquist et al.,[5] and Vorontsov et al.,[6] have demonstrated that the photoactivity of anatase nanoparticles is strongly particle size dependent. Anatase is one of the metastable phases (another known example is pure tetragonal or cubic ZrO_2 nanoparticles[7]) that can be fully stabilized into the nanoscale regime at ambient conditions and in the absence of stabilizer dopants. It is also a model compound that can provide information on the thermodynamics of phase transitions in many oxide materials driven by high-temperature coarsening.[8] Furthermore, as demonstrated in other nanoscale systems,[9,10] surface absorbents can play a significant role in the stabilization of nanophases and in the control of chemical reactions and properties. Consequently, obtaining anatase nanoparticles with high purity and precisely controlled particle size is key to understanding these important applications.

Anatase nanoparticles have been synthesized primarily by solution chemistries involving titanium sulfates and by hydrolytic reactions of titanium(IV) chloride or organic titanium.[11−13] These methods have shortcomings since chemical impurities or minor accessory phases are always present in the final

[†] Chinese Academy of Sciences.
[‡] Brigham Young University.

(1) Wells, A. F. *Structural Inorganic Chemistry*; Clarendon Press: Oxford, 1975.
(2) (a) O'Regan, B.; Gratzel, M. *Nature* **1991**, *353*, 737−740. (b) Kumar, K. N. P.; Keizer, K.; Burggraaf, A. J. *J. Mater. Chem.* **1993**, *3*, 1141−1149. (c) Ollis, D. F.; Pelizzetti, E.; Serpone, N. *Environ. Sci. Technol.* **1996**, *5*, 1522−1529.
(3) Nagaveni, K.; Sivalingam, G.; Hegde, M. S.; Madras, G. *Appl. Catal. B.* **2004**, *48*, 83−93.
(4) d'Hennezel, O.; Ollis, D. E. *Helv. Chim. Acta* **2001**, *84*, 3511−3518.
(5) Almquist, C. B.; Biswas, P. *J. Catal.* **2002**, *212*, 145−156.
(6) Vorontsov, A. V.; Altynnikov, A. A.; Savinov, E. N.; Kurkin, E. N. *J. Photochem. Photobiol.* A **2001**, *144*, 193−196.
(7) Roy, S.; Ghose, J. *Mater. Res. Bull.* **2000**, *35*, 1195−1203.
(8) Navrotsky, A.; Kleppa, O. J. *J. Am. Ceram. Soc.* **1967**, *50*, 626.
(9) Zhang, H.; Gilbert, B.; Huang, F.; Banfield, J. F. *Nature* **2003**, *424*, 1025−1029.
(10) Linsebigler, A. L.; Lu, G.; Yates, J. T. *Chem. Rev.* **1995**, *95*, 735−758.
(11) Sullivan, W. F.; Cole, S. S. *J. Am. Ceram. Soc.* **1959**, *42*, 127−133.
(12) (a) Gnanasekar, K. I.; Subramanian, V.; Robinson, J.; Jiang, J. C.; Posey, F. E.; Rambabu, B. *J. Mater. Res.* **2002**, *17*, 1507−1512. (b) Alemany, L. T.; Banares, M. A.; Pardo, E.; Martin-Jimenez, F.; Blasco, J. M. *Mater. Charact.* **2000**, *44*, 271−275. (c) Yang, J.; Mei, S.; Ferreira, J. M. F. *Mater. Sci. Eng., C* **2001**, *15*, 183−185. (d) Lao, C. F.; Chuai, Y. T.; Su, L.; Liu, X.; Huang, L.; Cheng, H. M.; Zuo, D. C. *Sol. Energy Mater. Sol. Cells* **2005**, *85*, 457−465. (e) Dhage, S. R.; Choube, V. D.; Samuel, V.; Ravi, V. *Mater. Lett.* **2004**, *58*, 2310−2313. (f) Wang, W.; Gu, B. H.; Liang, L. Y.; Hamilton, W. A.; Wesolowski, D. J. *J. Phys. Chem. B* **2004**, *108*, 14789−14792. (g) Pottier, A. S.; Cassaignon, S.; Chaneac, C.; Villain, F.; Tronc, E.; Jolivet, J. P.; *J. Mater. Chem.* **2003**, *13*, 877−882. (h) Vioux, A. *Chem. Mater.* **1997**, *9*, 2292−2299. (i) Arnal, P.; Coriu, R. J. P.; Leclercq, D.; Mutin, P. H.; Vioux, A. *Chem. Mater.* **1997**, *9*, 694−698. (j) Zhu, Y. F.; Zhang, L.; Gao, C.; Cao, L. L. *J. Mater. Sci.* **2000**, *35*, 4049−4054.
(13) Wang, C.; Ying, J. Y. *Chem. Mater.* **1999**, *11*, 3113−3120.

products. For example, a frequently employed method uses a sulfate process in which X-ray pure anatase can be obtained by adding a titanium sulfate solution into hot water under controlled conditions. This hydrolysis reaction on heating leads to anatase nanoparticles contaminated with 3 wt % sulfite species that are strongly bonded with the surfaces in a noncrystalline form and cannot be removed by washing.[11] Hydrolysis of $TiCl_4$ has extensively been reported for the synthesis of anatase nanocrystals at temperatures lower than 100 °C,[12d−g] but the formation reactions are sensitive to many factors such as pH, concentration in the reaction medium, molar ratio, and the types of mineralizers and additives (such as SO_4^{2-}, NH_4Cl, NaCl, $SnCl_4$, etc). The sum of these factors makes it very difficult to precisely control the particle size and compositions and to achieve high phase purity. In the case of organic hydrolytic reactions, TiO_2 nanoparticles obtained are crystallized primarily in the anatase phase but a minor phase of brookite cannot be eliminated by tuning the reaction conditions.[13] The presence of trace amounts of brookite has been reported to significantly enhance the transformation kinetics from anatase to rutile.[14a] Since impurities often appear during the formation of anatase nanoparticles, some have questioned[14−19] the inherent structural stability of anatase TiO_2 nanocrystals and the impact that might have on the application of anatase nanoparticles in photocatalytic reactions and many chemical processes.

The relevant questions, then, are as follows: (1) Can high purity anatase be synthesized without the accessory second phase of brookite or rutile?[13−17] (2) Do anatase nanoparticles contain OH^- groups as part of the lattice? (3) Does anatase become more stable in the nanoscale regime? (4) What are the hydrated surface characteristics of nanoanatase? Banfield et al.[18] performed a thermodynamic analysis and concluded that anatase becomes more stable relative to rutile at particle sizes smaller than approximately 14 nm. However, this conclusion may be drawn into question because systematic studies on size effects in *pure* anatase nanoparticles are unavailable and because there is poor knowledge about the surface hydration that is common to all nanoparticles. Recent work by our laboratory[20] and Park et al.[19] has clearly demonstrated the stability of rutile TiO_2 nanoparticles without traces of anatase to several nanometers when adopting suitable solution chemistries. For catalytic reactions, anatase nanoparticles have been found to show enhanced photocatalytic activity[21] and a maximum activity[5,6] at certain sizes when compared against commercial Degussa P-25 TiO_2. This has been explained in terms of particle size and the presence of large amounts of surface hydroxyl species.[5,6]

The relationship between particle size and the extent or size of the surface hydration layers is difficult to achieve since the assignment of OH^- groups on anatase surfaces still remains ambiguous.[22] Some OH stretching vibrations are observed between 3600 and 3800 cm^{-1} or 3350−3500 cm^{-1}, while some OH^- groups involved in hydrogen bonding have characteristic vibrations at about 3300 cm^{-1}. As a result, the type or the number of the OH^- groups are simply considered to depend on the sample origin and preparation conditions, which apparently underestimates the significance of the sample purity in assigning OH^- groups and in understanding the photocatalytic chemistry. Therefore, it is essential that a systematic study be performed on the synthesis of high purity anatase nanocrystals and on the control of the particle size due to grain growth kinetics. Until now, such a study has not been reported, most likely due to the difficulties associated with preparing pure phase anatase.

In this work, we prepared high purity anatase nanocrystals and explored the kinetic control of the particle size using a near room-temperature sol−gel technique in combination with high-temperature calcinations. We also examined several size-related structural features including surface hydration and lattice variations. The results that will be reported here will help explain the distinct properties of nanometer-sized anatase as compared to those of the bulk.

Experimental Section

Anatase nanocrystals were prepared using a sol−gel method with $TiCl_4$ (99.0% pure, Alfa Aesar) and ethanol (>97%, Aldrich Co.) as the starting materials. The preparation procedure is described as follows: 50 g of $TiCl_4$ was slowly added to 500 mL of ethanol at 0 °C in an ice−water bath. During the mixing process, a large quantity of yellowish gas, presumably EtCl and HCl, was released as a consequence of the predominant alcoholysis[12h] of $TiCl_4$ with ethanol and a partial hydrolysis of $TiCl_4$ with the residual water. After stirring at ambient conditions for 2 h, a transparent yellowish sol was formed which was then placed in an oven and baked at 87 °C for 3 days, producing an off-white powder. Just like many other non-hydrolytic sol−gel routes,[12h,i] the methodology reported in this work is ideal for crystallization of pure phase anatase nanocrystals since the main byproduct is EtCl which is volatile and can be removed by baking and the subsequent washings and, most importantly, the present formation reactions do not rely on hydrolysis for the creation of Ti−O bonds.

The off-white powder was washed carefully using a Beckman supercentrifuge at a speed of 25 000 rpm to remove organic species and Cl^- species that were adsorbed on the sample surfaces. The rinsing process was repeated several times a day for up to 60 days until the pH of the supernatant liquid reached 7, and the impurity concentrations were within the parts per million level. The white products thus obtained were dried at 50 °C in air and then found by X-ray diffraction to be the pure anatase phase. For the remainder of the paper, we denote this fully washed product as the as-is sample. It is important to note we found it necessary that the mixing of $TiCl_4$ with ethanol had to be performed at 0 °C and the gelling temperature had to be kept below 100 °C. If these conditions were not met, then (a) the as-is sample would contain a large portion of amorphous phases with the particle surfaces being covered by a carbon residue that hindered the crystallization of anatase nanoparticles on sintering[12j] or (b) the as-is sample would be in the rutile phase if the geling temperature was even as high as 110 °C.[12h]

To control the eventual grain size of the particles and to understand the grain growth kinetics, we investigated the final grain size of the particles as a function of calcination temperature and time. To study the dependence on calcination temperature, the as-is sample was put into an oven at selected temperatures in the range of 27−600 °C for a fixed period of 2 h. The time dependence was studied by keeping the as-is sample at 300 °C for varied reaction times from 2 to 48 h.

(14) (a) Overstone, J.; Yanagisawa, K. *Chem. Mater*. **1999**, *11*, 2770−2774. (b) Lee, D. S., Liu, T. K. *J. Sol−gel Sci. Technol*. **2002**, *25*, 121−136.
(15) Sugimoto, T.; Zhou, X. P. *J. Colloid Interface Sci*. **2002**, *252*, 347−353.
(16) Parala, H.; Devi, A.; Bhakta, R.; Fischer, R. A. *J. Mater. Chem*. **2002**, *12*, 1625−1627.
(17) Wilson, G. J.; Will, G. D.; Frost, R. L.; Montgomery, S. A. *J. Mater. Chem*. **2002**, *12*, 1787−1791.
(18) Zhang, H.; Banfield, J. F. *J. Mater. Chem*. **1998**, *8*, 2073−2076.
(19) Park, S. D.; Cho, Y. H.; Kim, W. W.; Kim, S. J. *J. Solid State Chem*. **1999**, *146*, 230−238.
(20) Li, G.; Li, L.; Boerio-Goates, J.; Woodfield, B. F. *J. Mater. Res*. **2003**, ***18***, 2664−2669.
(21) Nagaveni, K.; Sivalingam, G.; Hedge, M. S.; Madras, G. *Appl. Catal. B* **2004**, *48*, 83−89.
(22) (a) Busca, G.; Saussey, H.; Saur, O.; Lavalley, J. C.; Lorenzelli, V. *Appl. Catal*. **1985**, *14*, 245−260. (b) Morterra, C. *J. Chem. Soc., Faraday Trans*. **1988**, *84*, 1617−1637.

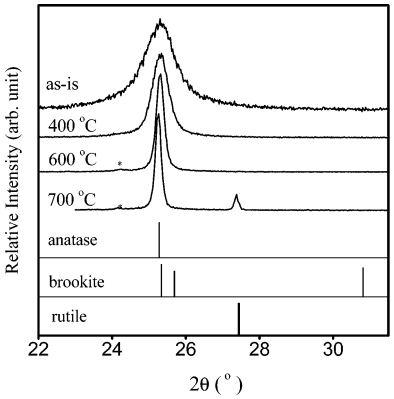

Figure 1. XRD patterns for the as-is anatase nanoparticles of 7.7 nm in size as prepared by a modified sol−gel method after baking at 87 °C and for the samples after calcinations at selected temperatures for 2 h. Symbol ∗ denotes the secondary diffraction of tungsten in the target chamber. Vertical bars below the patterns represent the standard diffraction data from JCPDS file for anatase (No. 21-1272), brookite (No. 29-1360), and rutile (No. 21-1276).

The structures of all samples were identified by powder X-ray diffraction (XRD) at room temperature on a Scintag diffractometer (copper target) at a scanning rate of 0.5°/min at a power of 12 kW. The lattice parameters for the samples were refined by least-squares methods with nickel powder (99.99%) being used as the internal standard for peak position calibrations. The average grain sizes (D) were calculated from the most intense diffraction peak (110) using the Scherrer formula:

$$D = \frac{0.9\lambda}{\beta \cos \theta}$$

where λ is the X-ray wavelength employed, θ is the diffraction angle of the (110) peak, and β is defined as the half-width after subtracting for the instrumental broadening.

The morphology and particle size of the samples were examined by transmission electron microscopy (TEM) on a JEOL JEM 2000-FX instrument under an acceleration voltage of 200 keV. The chemical compositions were examined with a scanning electron microscope (Philips) that is equipped with an energy-dispersive X-ray spectrometer (EDX) analyzer. A careful elemental analysis for low levels of carbon and chlorine was performed at Galbraith Laboratories, Inc., in Knoxville, TN, using a combustion method.

The surface species were studied by determining the binding energies of the O 1s and Ti 2p core electrons using X-ray photoelectron spectroscopy (XPS) (VG Eclipse 220i-XL) that was performed with a monochromatic Al Kα X-ray source and with an electron takeoff angle of 90°. During the measurements, the base pressure of the sample chamber was kept at 10^{-10} Pa. The binding energy data are obtained using the instrument software and emission line calibration with the C1s signal at 284.6 eV.

Thermal analysis was performed using simultaneous differential scanning calorimetry and thermogravimetric analysis (TGA) using a Netzsch 409. The measurements were performed at a heating rate of 10 °C/min from room temperature to 1000 °C in an argon atmosphere at a flux of 40 mL/min. The infrared (IR) spectra of the samples were recorded using a KBr pellet technique. Precautions of (i) drying the KBr powders under infrared lamp for 2 h before pressing pellet and (ii) subtracting the background signals have been taken to ensure that spectra recorded are not from the atmospheric water and/or carbonates.

Results and Discussion

1. Formation of High Purity Anatase Nanoparticles. Figure 1 shows the enlarged XRD patterns over a scan interval from 22° to 31.5° for the as-is sample and the samples prepared after heating the as-is sample at 400, 600, and 700 °C, respectively, in air for 2 h. The standard diffraction data over the same scan interval for anatase, rutile, and brookite are also given for phase composition determinations. It is seen that the XRD data for the samples obtained at temperatures lower than 600 °C match the standard anatase pattern (JCPDS 21-1272), and there is an absence of weak diffraction peaks at 27° or 31°, indicating that the samples are free of rutile and brookite TiO_2. All diffraction peaks are highly symmetric and fitted as single peaks by Lorentzian functions. Our Raman spectra did not show any traces of brookite or rutile but a systematic shift in frequencies that are to be described elsewhere. In view of the detection limit for brookite of 3.1% by XRD[23a] and much less than 0.5% by Raman,[23b] these combined results demonstrate the formation of single-phase anatase.

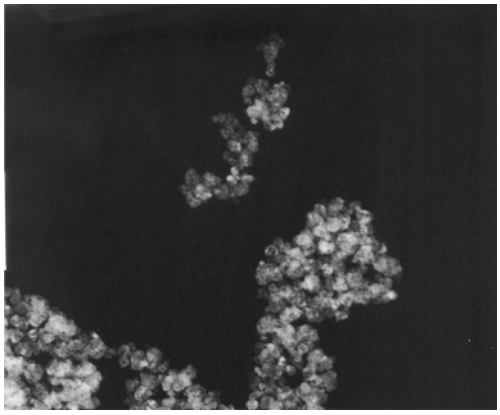

Figure 2. A TEM photo of 16 nm anatase that was prepared after heating the as-is sample at 400 °C for 2 h.

From Figure 1, it is clear that the samples prepared at calcination temperatures lower than 600 °C show broadened diffraction peaks. Similar broadening effects have also been found for the anatase samples that were obtained using shorter calcination times. We adopted the Williamson and Hall method[24] to distinguish the contributions of internal strain and particle size to the peak broadening. We found that the internal strains in these anatase nanocrystals were extremely small. Therefore, the particle size was calculated by peak broadening and further confirmed by TEM. Figure 2 shows a TEM photo for 16 nm anatase that was prepared after heating the as-is sample at 400 °C for 2 h. The anatase nanoparticles are seen to have a spherical shape. The diameters of the particles determined by TEM are nearly the same as the average particle size calculated from XRD peak broadening. Consequently, we use the average particle sizes calculated by peak broadening to describe the grain growth kinetics of anatase nanocrystals.

Our experiments show that anatase nanoparticles are smaller at lower calcination temperatures, and we also found that all diffraction peaks in Figure 1 for the anatase phase had a small but systematic shift toward higher angles with decreasing calcination temperature. The lattice parameters of our anatase particles were determined using a standard least-squares method. Figure 3 shows the particle size dependence of the lattice volume $V(= a^2c)$ where a and c denote the lattice parameters of the tetragonal unit cell. It is clearly seen that the lattice volume

(23) (a) Mogyorosi, K.; Dekany, I.; Fendler, J. H. *Langmuir* **2003**, *19*, 2938−2946. (b) Murad, E.; Koster, H. M. *Clay Minerals* **1999**, *34*, 479−485.
(24) Williamson, G. K.; Hall, W. H. *Acta Metall.* **1953**, *1*, 22−25.

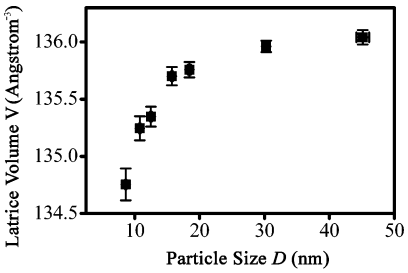

Figure 3. Relationship between the particle size and lattice volume of anatase nanoparticles.

decreases with decreasing particle size. This result is completely opposite to the lattice expansions that have been frequently observed in many nanoscale oxides such as CeO_2,[25] MgO,[26] Fe_2O_3,[27] and rutile TiO_2,[28] although a lattice contraction with decreasing particle size seems reasonable from a thermodynamic viewpoint due to the higher surface curvature as is observed in non-oxide nanocrystalline metals such as Si, ZnS, and CdSe.[29] Conceivably, in the nanoscale regime, valence reduction might occur causing lattice variations as is observed in CeO_2 nanoparticles.[25] Our electron paramagnetic resonance (EPR) measurements (not shown), however, do not show any evidence of Ti^{3+} in our anatase nanoparticles, which eliminates the possibility of oxidation as a source of the lattice variations since the detection limit of Ti^{3+} by the EPR technique can be as low as 0.1 at. %.[30] Water adsorbed on the surfaces has also been suggested as the cause for the lattice expansion in nanoparticles such as in MgO.[26] This explanation appears to be supported by our recent results on rutile TiO_2 nanorods[28] in which we discovered a lattice expansion in the presence of large quantities of adsorbed water. As described later, our anatase nanoparticles also have highly hydrated surfaces.

There are two dominant phenomena governing the change in lattice volume as the particle size is reduced. The first is surface stresses (such as hydration chemistry) which can create a positive pressure that in turn produces a lattice contraction, while the other originates from the long-range repulsive interactions of the parallel surface defect dipoles[28] that are produced when the titanium atoms shift toward the coordinated oxygen atoms at the surfaces by yielding negative pressures responsible for a lattice expansion. As indicated by a theoretical calculation using an ab initio method,[31] the anatase lattice has a small polarizability, consequently the surface defect dipoles accumulated from the lattice polarization become very low and the repulsive interactions of the parallel surface defect dipoles[28] accounting for the negative pressure on the anatase nanocrystals become weak. Therefore, we conclude that the net positive pressure, seemingly caused by the large surface hydration, is the primary reason that anatase nanocrystals have a smaller equilibrium volume than that of the bulk phase. Therefore, the presence and explanation of a lattice contraction in anatase nanocrystals, in contrast to the lattice expansion in other nanosized oxides,[25−28] provides additional insight into nanostructured oxides in general and may have broad scientific and technological implications, a discussion of which is beyond the scope of this paper. However, several important papers address these topics.[32−34]

One of the important features we have observed for anatase nanoparticles is a size-induced phase transition. When the calcination temperature was higher than 700 °C, as seen in Figure 1, a weak diffraction peak appeared at about 27°, which is associated with the partial transformation of anatase to rutile. With increasing calcination temperature, the relative content of rutile grew significantly at the expense of the anatase phase. The critical size for the transition of anatase to rutile in our system is somewhere between 32 and 42 nm, and the critical temperature for our phase pure anatase is intermediate between 600 and 700 °C. Gribb and Banfield[35] studied the particle size effects on the transformation kinetics of anatase to rutile in TiO_2 nanoparticles that were prepared by hydrolytic reactions of titanium isopropoxide. Their results showed that when the particle sizes are beyond 10 nm and heat treatment temperatures are higher than 525 °C, the rutile phase would begin to appear. Apparently, the critical size and transformation temperature are much smaller or lower than those for our high purity nanoanatase samples. Considering that the anatase nanoparticles by hydrolytic reactions of the titanium organic systems are generally contaminated by organic absorbents and/or the accessory brookite phase,[36,37] and that the adsorbed alcohol species and traces of brookite might accelerate the anatase−rutile transition by drastically decreasing the transition temperatures,[36,38] we believe that with high purity surfaces, interparticle sintering can be reduced.

Chemical analysis of our as-is sample of 7.7 nm by EDX indicated the presence of titanium and oxygen only. Our trace analysis by combustion methods gave the chemical compositions of 1.25 wt % H, and 165 ppm Cl. Structural refinements of our pure anatase phase samples by the Rietveld method using Rietica program[39] indicate a tetragonal structure. These results show that our as-is sample is chemically pure with the stoichiometry of $TiO_2 \cdot 0.55\ H_2O$ at ambient conditions. The presence of higher concentrations of hydrogen at small sizes is associated with the surface hydration effects that will be described later. The extremely low concentration of Cl^- species in our anatase nanoparticles shows that this synthetic route, with sufficient rinsing, is superior over other preparation methods in obtaining high purity anatase nanoparticles. Sullivan and Cole[11] studied the hydrolysis of titanium sulfate solutions and obtained X-ray

(25) Tsunekawa, S.; Ishikawa, K.; Li, Z. Q.; Kawazoe, Y.; Kasuya, A. *Phys. Rev. Lett.* **2000**, *85*, 3440−3443.
(26) Cimino, A.; Porta, P.; Valigi, M. *J. Am. Ceram. Soc.* **1966**, *49*, 152−156.
(27) Ayyub, P.; Palkar, V. R.; Chattopadhyay, S.; Multani, M. *Phys. Rev. B* **1995**, *51*, 6135−6138.
(28) Li, G.; Boerio-Goates, J.; Woodfield, B. F.; Li, L. *Appl. Phys. Lett.* **2004**, *85*, 2059−2061.
(29) (a) Taneda, A.; Kawazoe, Y. *J. Magn. Soc. Jpn.* **1999**, *23*, 679. (b) Ji, Y. L.; Guo, L.; Xu, H. B.; Liu, J.; Li, X. D.; Li, Y. C.; Wu, Z. Y.; Simon, P.; *Phys. Status Solidi A* **2003**, *198*, 210−214. (c) Yu, D. K.; Zhang, R. Q.; Lee, S. T. *Phys. Rev. B* **2002**, *65*, 245417. (d) Sarangi, S. N.; Sahu, S. N. *Physica E* **2004**, *23*, 159−167. (e) Zhang, J. Y.; Wang, X. Y.; Xiao, M.; Qu, L.; Peng, X. *Appl. Phys. Lett.* **2002**, *81*, 2076−2078.
(30) (a) Swider, K. E.; Worrell, W. L. *J. Am. Ceram. Soc.* **1995**, *78*, 961−964. (b) Merino, R. I.; Orera, V. M.; Lomonova, E. E.; Batygov, S. K. *Phys. Rev. B* **1995**, *52*, 6150−6153.
(31) Cangiani, G. Ph. D. Thesis, University of Trieste, Italy, 2003.
(32) Kelley, S.; Pollak, F. H.; Tomkiewicz, M. *J. Phys. Chem. B* **1997**, *101*, 2730−2734.
(33) Ranade, M. R.; Navrotsky, A.; Zhang, H. Z.; Banfield, J. F.; Elder, S. H.; Zaban, A.; Borse, P. H.; Kulkarni, S. K.; Doran, G. S.; Whitfield, H. J. *Proc. Natl. Acad. Sci. U.S.A.* **2002**, *99*, 6476.
(34) (a) Fernandez-Garcia, M.; Martinez-Arias, A.; Hanson, J. C.; Rodriguez, J. A. *Chem. Rev.* **2004**, *104*, 4063−4104. (b) Murty, B. S.; Datta, M. K.; Pabi, S. K. *Sadhana Acad. Proc. Eng. Sci.* **2003**, *28*, 23−45.
(35) Gribb, A. A.; Banfield, J. F. *Am. Mineralogr.* **1997**, *82*, 717−728.
(36) Ha, P. S.; Youn, H. J.; Jung, H. S.; Hong, K. S.; Park, Y. H.; Ko, K. H. *J. Colloid Interface Sci.* **2000**, *223*, 16−20.
(37) Lee, S. J.; Lee, C. H. *Mater. Lett.* **2002**, *56*, 705−708.
(38) Hu, Y.; Tsai, H. L.; Huang C. L. *J. Eur. Ceram. Soc.* **2003**, *23*, 691−696.
(39) Kutty, T. R. N.; Vivekanandan, R.; Murugaraj, P. *Mater. Chem. Phys.* **1998**, *19*, 533−546.

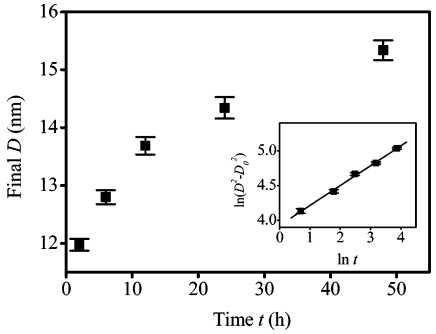

Figure 4. Isothermal grain growth for anatase nanocrystals that were obtained at 300 °C for different reaction times. Inset shows the grain growth plotted as $\ln(D^2 - D_0^2)$ versus t. D_0 denotes the initial particle size.

pure anatase; however, the surfaces of their anatase samples contained a significant impurity concentration of 3 wt % sulfite species that is difficult to remove completely. Generally, the ionic species present during the synthesis play a significant role in the phase formation of the final products; different phases are produced depending on the chemical nature of these species. High concentrations of Cl^- species leads to the rutile,[20] while SO_4^{2-} results in anatase.[39] Our reaction systems have involved high concentrations of Cl^-; however, the final product is highly chlorine free and also rutile or brookite phase free. These results can be explained by the formation, during the mixing processes of $TiCl_4$ and ethanol, of an intermediate product $TiCl_x(OCH_2CH_3)_{4-x}$ whose structural units are similar to the anatase lattice.[12j]

During the reactions, the presence of complexes on the surface of the freshly formed anatase nanoparticles would play a dominant role in the particle growth by preventing the agglomeration of the particles. This has been indicated by our TEM observations in Figure 2 where all the nanoparticles are homogeneously distributed and individual shapes are seen. Finally, it should be noted that the as-is anatase of 7.7 nm was obtained by baking at 87 °C, which allows size tailoring of anatase nanoparticles for kinetic and structural studies and many other applications. Lower temperature synthetic routes for the formation of nanosized anatase have been reported but for each it is difficult to achieve small sizes with high purity.[40] Nam et al.[40a] reported the synthesis of anatase nanocrystals in a very narrow temperature range of 65−100 °C by controlling the hydrolysis of $TiCl_4$ in aqueous solutions. However, Zhang et al.[40b] and Cheng et al.[40c] using similar conditions, demonstrated that pure anatase phase can be only obtained in the presence of a small amount of sulfate species or at a hydrothermal reaction temperature of 200 °C with pH > 7. Otherwise a mixture of anatase and rutile will be readily formed because the hydrolysis of $TiCl_4$ in aqueous solution is more kinetically favorable for rutile than anatase.[40d] This reinforces that our methodology is well suited for low-temperature synthesis of highly dispersed and crystallized anatase nanoparticles with high purity.

2. Grain Growth Kinetics. Figure 4 shows the isothermal grain growth of anatase nanocrystals obtained at 300 °C for different calcination times, t. The particle size, D, of anatase nanocrystals increased from 12 to 15.3 nm when the calcination

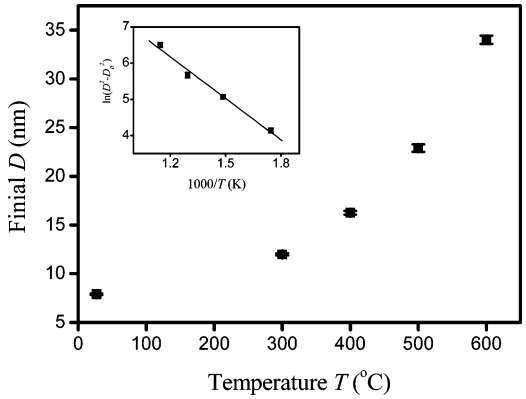

Figure 5. Temperature dependence of the particle size for anatase nanocrystals that were obtained after heating at different temperatures for 2 h. Inset shows the grain growth plotted as $\ln(D^2 - D_0^2)$ versus $1/T$.

time was increased from 2 to 48 h. Shown in the inset of Figure 4 is a log−log plot of t versus $D^2 - D_0^2$, where D_0 denotes the initial particle size of the as-is sample. The relationship between D and t was found to follow the linear equation

$$\ln(D^2 - D_0^2) = 3.93(2) + 0.286(9)\ln t \qquad (3)$$

where, here and in what follows, the digits in parentheses represent the error bars.

Shown in Figure 5 is the temperature dependence of the particle size for anatase nanocrystals obtained after heating the as-is sample at different temperatures with a fixed calcination time of 2 h. It is seen that with increasing calcination temperature, the particle size of anatase nanocrystals increased from approximately 7.7 nm at room temperature to 32 nm at 600 °C. The inset in Figure 5 shows the same data but graphed as $\ln(D^2 - D_0^2)$ versus $1/T$. As is clearly shown, there also exists a linear relationship between $\ln(D^2 - D_0^2)$ and $1/T$ of the form,

$$\ln(D^2 - D_0^2) = 10.8(4) - \frac{3.8(3) \times 10^3}{T} \qquad (4)$$

Combining the isothermal and temperature-dependent grain growth equations (eqs 3 and 4) would allow us to better understand the grain growth kinetics via the calculation of the grain growth exponent and activation energy. The grain growth kinetics of TiO_2 nanoparticles have been investigated previously and exhibit several different expressions depending on the growth mechanisms, reaction routes, and the final phases.[20,41] Liu et al.[42] studied the grain growth kinetics of impure TiO_2 nanoparticles (with organic absorbents and traces of rutile as justified latter) and yielded a grain growth kinetics of $D^n = k_0 t^m e^{-E_a/RT}$ with a growth exponent of $n = 5$ for anatase TiO_2 nanoparticles and $n = 2$ for the rutile TiO_2 nanoparticles, which were obtained after heating the impure anatase nanoparticles at temperatures higher than 550 °C. Our earlier work on rutile nanoparticles prepared directly from hydrothermal conditions[20] gave a grain growth kinetics that can be well described using the equation $D^n = k_0 t e^{(-E_a/RT)}$ with a growth exponent of $n = 5$. Comparatively, for TiO_2 nanoparticles prepared using a high-

(40) (a) Nam, H. D.; Lee, B. H.; Kim, S. J.; Jung, C. H.; Lee, J. H.; Park S. *Jpn. J. Appl. Phys. I* **1998**, *37*, 4603−4608. (b) Zhang, Q. H.; Gao, L.; Guo, J. K. *J. Eur. Ceram. Soc.* **2000**, *20*, 2153−2158. (c) Cheng, H. M.; Ma, J. M.; Zhao, Z. G.; Qi, L. M. *Chem. Mater.* **1995**, *7*, 663−671. (d) Li, Y. Z.; Fan, Y.; Chen, Y.; *J. Mater. Chem.* **2002**, *12*, 1387−1390.

(41) Trentler, T. J.; Denler, T. E.; Bertone, J. F.; Agawal, A.; Colvin, V. L. *J. Am. Chem. Soc.* **1999**, *121*, 1613−1614.

(42) Liu, H. Z.; Hu, W. B.; Gu, M. Y.; Wu, R. J. *Wuji Cailiao Xuebao* **2002**, *17*, 429−436.

temperature sintering process,[43] the grain growth kinetics are represented using a growth exponent of $n = 2$.

In this work, different sizes of anatase nanoparticles were achieved using high-temperature calcinations; therefore, we have assumed that the kinetic grain growth exponent is $n = 2$ and the growth kinetics of the anatase nanocrystals will follow the equation

$$D^n = D_0{}^n + k_0 t^m e^{(-(E_a/RT))} \quad (5)$$

where D is the particle size at time t and temperature T, D_0(= 7.7 nm) is the initial particle size, m is the time exponent, k_0 denotes a preexponential constant, E_a is the activation energy for grain growth, and R is the gas constant.

For isothermal grain growth, the particle size, D, is solely a function of time, t. Therefore, eq 5 can be rewritten as follows

$$\ln(D^2 - D_0{}^2) = m \ln t + C_1 \left(C_1 = \ln k_0 - \frac{E_a}{RT}\right) \quad (6)$$

where it is easily seen that eq 6 has the same form as eq 3. Consequently, the kinetic grain growth exponent can be extracted as $m = 0.286 \pm 0.009$ by comparison with eqs 3 and 6.

For the temperature-dependent grain growth, the reaction time is fixed as a constant, $t = 2$ h, and the particle size is only a function of temperature. Equation 5 can be rewritten as

$$\ln(D^2 - D_0{}^2) = C_2 - \frac{E_a}{RT} (C_2 = \ln(k_0 t^m)) \quad (7)$$

Therefore, the activation energy for grain growth can be obtained by combining eqs 4 and 7 and by using the exponent $m = 0.286 \pm 0.009$ that has been determined using the isothermal grain growth in eq 6. The value obtained for the activation energy is $E_a = 32 \pm 2$ kJ·mol^{-1}. Consequently, the grain growth kinetics of anatase nanocrystals can be described using the full growth kinetics equation

$$D^2 = D_0{}^2 + 3.86 \times 10^4 \times t^{0.286(9)} e^{(-32(2)/RT)} \quad (8)$$

Equation 8 is important since it helps us better understand the growth mechanism by revealing the parameters that control the grow kinetics. It is seen from eq 8 that the activation energy of our anatase nanoparticles is $E_a = 32 \pm 2$ kJ·mol^{-1}. Comparatively, Liu et al.[42] reported $E_a = 39 \pm 6$ kJ/mol for the anatase nanoparticles at temperatures lower than 823 K. The difference in activation energy can be explained in terms of the methodology and the growth kinetic model that had been adopted. Liu et al.'s anatase nanoparticles[42] were prepared by a microemulsin-mediated reaction of $TiCl_4$, a method that is most likely to introduce a minor phase of rutile in final anatase nanoparticles.[44] The larger activation energy reported by Liu et al. is thus associated with the minor phase of rutile which has an activation energy much larger than that for anatase nanoparticles. For example, E_a for rutile nanoparticles can be as large as 170.8 kJ·mol^{-1} or 230 kJ·mol^{-1} depending on the preparation methods.[20,43] On the other hand, unsuitable assumptions in the growth kinetics can also contribute to the variations in the activation energy. Liu et al.,[42] obtained their activation energies of anatase nanoparticle at lower temperatures using eq 5 with assumptions of $n = 5$ and $D^5 \ll D_0$.[5] These assumptions cannot be realistic since the particle sizes at lower temperatures are not that different from their initial size. As a result, the underestimated size terms could yield a larger E_a. It is clear, then, that the activation energy for our high purity anatase nanoparticles is currently the most reliable. Since our activation energy is close to that of $E_a = 40$ kJ·mol^{-1} for proton transfer along hydrogen bonds in forming ionized molecular species,[45] it is plausible that the mechanism for grain growth of the anatase nanocrystals is via a transfer process of the hydration species such as $TiO_2 \cdot nH_2O$ to the adjacent anatase nanoparticles which in turn stimulates growth by a combination reaction. The highly activated surface hydration layers can act as an effective passage for the transfer and will be described in the following section.

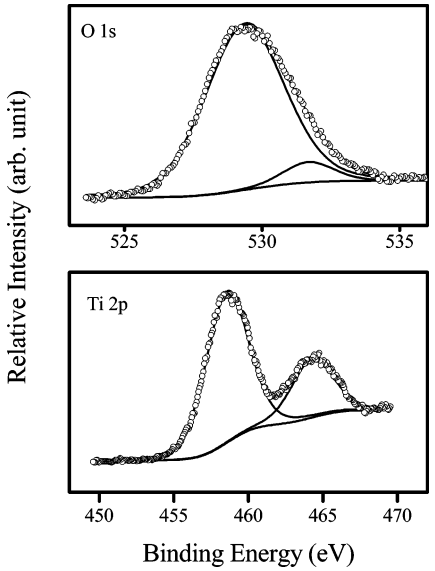

Figure 6. Core level photoemission spectra of O 1s and Ti 2p for 7.7 nm anatase nanoparticles.

3. Hydration Effects. Figure 6 shows typical O 1s and Ti 2p core level spectra obtained on 7.7 nm anatase. Data fit using the analytical software in the measurement apparatus showed that the O 1s spectrum in Figure 6 consists of a strong photoelectron signal around 530.0 eV and a shoulder around 532.2 eV. The O 1s signal at approximately 530.0 eV is assigned to the bulk oxygen (O^{2-}), while that at approximately 532.2 eV is assigned to the surface water adsorbed on the sample surface.[46] For Ti 2p core level spectrum in Figure 6, all Ti 2p signals are highly symmetric, and no shoulders were observed on the lower energy sides of the strong Ti 2p signals. These results show that the defect concentration associated with Ti^{3+} is extremely low.[20]

The hydration effect is also examined using TGA analysis. As shown in Figure 7, the mass loss for 7.7 nm anatase occurs in a wide temperature range from room temperature to 400 °C. It should be noted that the relative mass is almost an exponential decay from temperature lower than 100 °C to those above 300 °C. The distinct mass loss at temperatures lower than 100 °C indicates the presence of free water or physisobed water, while

(43) Hofler, H. J.; Averback, R. S. *Scr. Metall. Mater.* **1990**, *24*, 2401−2407.
(44) Wu, M.; Long J.; Huang, A.; Luo, Y.; Feng, S.; Xu, R. *Langmuir* **1999**, *15*, 8822−8825.
(45) Collier, W. B.; Ritzhaupt, G.; Devlin, J. P. *J. Phys. Chem.* **1984**, *88*, 363−368.
(46) Kim, K. S.; Winograd, N. *Surf. Sci.* **1974**, *43*, 625−643.

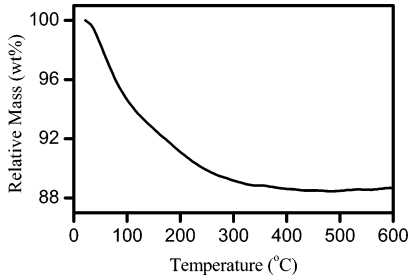

Figure 7. TGA curve for 7.7 nm anatase measured in a flow of Ar gas.

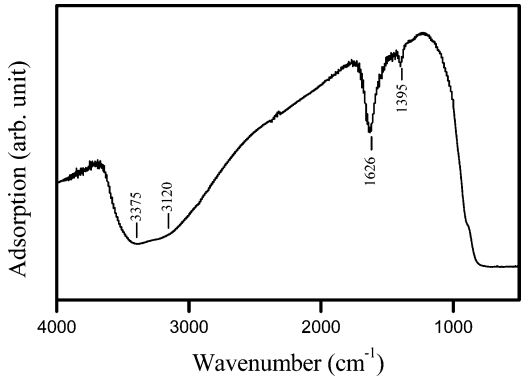

Figure 8. IR spectrum for 7.7 nm anatase measured using a KBr pellet technique.

the continuous decay of relative mass vs temperature suggests that, for our pure anatase samples, the surface water molecules most likely exist in a wide set of energetically nonequivalent surface hydration groups. Also, the water content for the 7.7 nm anatase reached as high as 11 wt %. The large hydration sphere, however, was found to decrease with increasing particle size and calcination temperature.

The OH^- bonding characteristics of the water molecules associated with the surface hydration layer were examined by IR spectroscopy. Since the signals of CO_2 and H_2O in air have already been subtracted, the IR data in Figure 8 represent the characteristic absorbance of our high purity anatase nanoparticles. For 7.7 nm anatase, as shown in Figure 8, two strong, broad absorptions centered around 3375 and 3120 cm^{-1}, a weak sharp absorption band at about 1626 cm^{-1}, and a very weak absorption at 1395 cm^{-1} were observed. The absorption located at 3375 cm^{-1} characterizes the hydroxyl groups of Ti−OH at weak surface active sites with which physisorbed water molecules are bound by weak hydrogen bonds with OH^- groups of TiO_2 surfaces,[47] while the absorption at 3120 cm^{-1} is associated with water complexes that are strongly bound to the TiO_2 surface. The weak adsorption at 1626 cm^{-1} is associated with the deformation vibration for H−O−H bonds of the physisobed water. Fitting the integral intensities for the OH^- vibrations in the range of 3100 to 3400 cm^{-1} by Lorentzian functions indicates that the as-is anatase has approximately 75% of the surface hydration layer in "strong" adsorption centers and about 25% in "weak" adsorption centers. The strong adsorption centers are active to CO_2 in the atmosphere, which accounts for the appearance of the very weak adsorption band at 1395 cm^{-1} for CO_3^{2-} and HCO_2^{3-} ions.[48] These results are

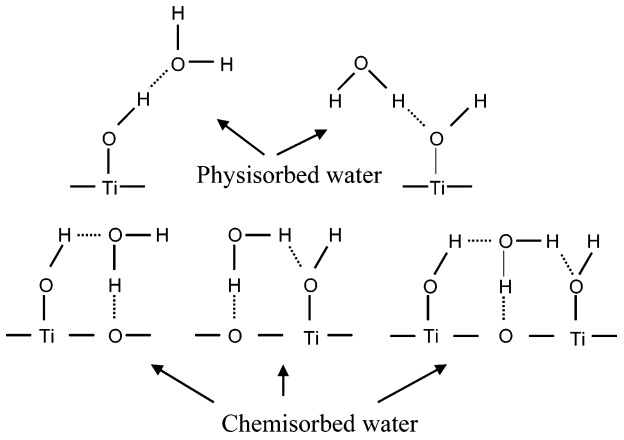

Figure 9. Structures proposed for the hydration sphere for anatase nanoparticles.[50]

consistent with our TGA measurements in which the hydration sphere is shown to be very large for small sizes. On the other hand, in Figure 8, the absorption bands associated with the isolated OH^- group vibrations were not observed around 3665 and 3715 cm^{-1}, which indicates a high degree of hydration on the anatase surfaces.

It should also be noted that the sharp, doublet absorption bands at 3277 and 3322 cm^{-1} associated with the lattice hydroxyls are very weak. These results indicate that for our pure anatase nanoparticles, OH^- species do not occupy the lattice sites. Structural OH^- species have previously been reported in the synthetic and natural TiO_2 rutile crystals.[49] Incorporation of OH^- groups usually happens around the defect sites of Ti^{3+} or other low valence ions due to the requirements of charge balance. However, our XPS measurements, as indicated in Figure 6, do not show any evidence for Ti^{3+}. Water molecules on the surface may interact with the surface titanium ions and/or lattice oxygen through structures[50] illustrated in Figure 9. It is known that the nanoparticles have an abundance of dangling bonds at the surfaces due to the unsaturated coordination of titanium. These dangling bonds might form defect dipoles perpendicular to the outer surfaces[28] as a consequence of surface hydration in the presence of polar hydroxyl groups and strong electron-acceptor centers; i.e., the coordinatively unsaturated Ti^{4+} ions. This hydrated surface structure in Figure 9 is therefore stabilized by the hydrogen bonds with the coordinated oxygen of anatase lattice and/or the adjacent bridging OH^- groups. Anatase nanoparticles have surfaces of significant nonhomogeneity:[31] different crystal planes and various types of surface defects have been observed on their surfaces. So, hydration with these active centers can be expected to lead to a wide set of energetically nonequivalent surface groups, accounting for the continuous dehydration to high temperatures.

On the other hand, during the dehydration at temperatures higher than 100 °C, hydrogen bonds linking the chemisorbed water molecules with the lattice oxygen or adjacent OH^- groups would be recombined by transforming weaker hydrogen bonds into stronger bonds, which has been further evidenced by the continuous mass loss at $T > 100$ °C in Figure 7 as well as a linear size dependence of dehydration amount to be described elsewhere. Therefore, the rearrangement of the hydrogen bonds

(47) Bezrodna, T.; G. Puchkovska, G.; Shimanovska, V.; Chashecnikova, I.; Khalyavka, T.; Baran, J. *Appl. Surf. Sci.* **2003**, *214*, 222−231.
(48) Li, X.; Liu, H.; Wang, J.; Cui, H.; Zhang, X.; Han, F. *Mater. Sci. Eng., A* **2004**, *379*, 347−350.
(49) Dennis, P. F.; Freer, R. *J. Mater. Sci.* **1993**, *28*, 4804−4810.
(50) Bezrodna, T.; Puchkovska, G.; Shymanovska, V.; Baran, J.; Ratajczak, H. *J. Mol. Struct.* **2004**, *700*, 175−181.

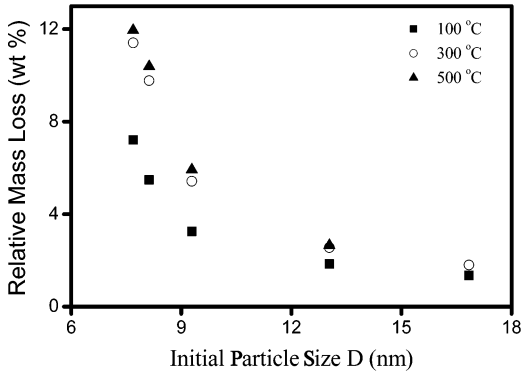

Figure 10. Size dependence of the mass loss for anatase nanoparticles at the indicated temperatures.

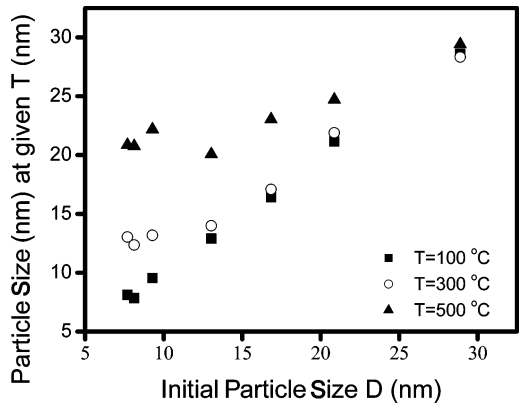

Figure 11. The final particle sizes after heating the initial anatase nanoparticles at given temperatures in air for 2 h.

as well as the resulting polar fields could impose strong influences on the particle sizes by modifying the ionic hydration species in diffusion for grain growth.

Figure 10 shows the weight-loss dependence on the initial sizes for anatase nanoparticles at a given temperature. It can be seen that at high temperatures, all anatase nanoparticles yield large mass losses due to dehydration. Such a thermal process is followed by grain growth since, as indicated by our growth kinetics described above, anatase nanoparticles became larger with increasing calcination temperatures. The weight losses in Figure 10 indicate that the smaller particle sizes have more adsorbed water while larger particle sizes have less. Therefore, surface hydration molecules can be an important component of the anatase nanoparticles, which likely balance the increased lattice energy when anatase particles become smaller. To confirm this assumption, we heated the anatase nanoparticles at different temperatures and measured the particle sizes. Figure 11 illustrates our mapping results on the final sizes after calcinations at the indicated temperatures for 2 h. Note that the anatase nanoparticles at 100 °C did not show any significant changes in sizes from the as-is sample. This result is important since the treatment at 100 °C can significantly reduce the water content while keeping the particle size small. This phenomenon can be explained by the weak hydrogen bonds associated with the physisorbed water as illustrated in Figure 9. We have taken advantage of this hydration feature and successfully extracted the pronounced contributions of the surface hydration layer to the heat capacity of the various TiO_2 phases, which will be described elsewhere. It is also seen from Figure 11 that with increasing calcination temperature, smaller anatase nanoparticles will become considerably larger. These results strongly demonstrate that the chemisorbed water can be a dominant component in stabilizing the small sizes of the nanoparticles, and removal of the surface hydration layer will lead to coarsening of the nanoparticles.

Conclusions

The main results reported in this work are summarized as follows:

(1) High purity anatase nanoparticles were prepared via a modified sol−gel method by mixing $TiCl_4$ with ethanol and a subsequent calcination process. This reaction route eliminated the formation of the brookite phase that is usually observed in other low-temperature reaction methods.

(2) The particle sizes of anatase nanoparticles are found to be well controlled by reaction temperature and time. The grain growth kinetics for anatase nanoparticles can be described using the equation,

$$D^2 = D_0^2 + 3.86 \times 10^4 \times t^{0.286(9)} e^{(-32(2)/RT)}$$

(3) Anatase nanocrystals have a large hydration sphere whose size is a function of particle size. IR measurements indicate that for the hydration layer, the OH^- species are not an integral part of the lattice but on the surfaces by hydrogen bonds with a wide set of energetically nonequivalent surface hydroxyl groups.

(4) Surface hydration is revealed to be an important component of anatase nanoparticles and plays a dominant role in keeping the fine nature of the nanoparticles. Heating hydrated particles at 100 °C for 2 h allows for the removal of a small amount of water with only a small increase in particle size. Removal of surface water below a certain threshold value, whose magnitude increases with decreasing particle size, leads to significant grain growth.

Acknowledgment. This work was financially supported by a grant from the Department of Energy (USA) under contract numbered DE-FG03-01ER15235 and, in part, by a grant from the Hundreds Youth Talents Program of the Chinese Academy of Science (Li G). We thank Professors Alexandra Navrotsky, University of California at Davis, and Frances Hellman, University of California at Berkeley, for many fruitful discussions as part of our ongoing collaboration. We also appreciate the assistance of Marcus Donaldson and Sarah Doot Hopkins with the significant number of sample washings that were required in this project. The authors express their thanks to Dr. M. R. Linford and Mr. Guilin Jiang for help in the X-ray photoelectron spectroscopy measurements.

JA050517G